

Supplementary Materials for

MoS₂ pixel arrays for real-time photoluminescence imaging of redox molecules

M. F. Reynolds, M. H. D. Guimarães, H. Gao, K. Kang, A. J. Cortese, D. C. Ralph, J. Park, P. L. McEuen*

*Corresponding author. Email: plm23@cornell.edu

Published 8 November 2019, *Sci. Adv.* **5**, eaat9476 (2019)

DOI: 10.1126/sciadv.aat9476

The PDF file includes:

Supplementary Materials and Methods

Fig. S1. Characterization of MoS₂ samples.

Fig. S2. Diagram of the experimental setup.

Fig. S3. Detection of ions in solutions containing ruthenocene and ruthenocene/ferrocene mixtures.

Fig. S4. Diffusion current mapping of ferrocene ions.

Fig. S5. PL decay time for varied Fc concentrations.

Fig. S6. PL imaging of electroosmotic flow.

Fig. S7. PL versus dopamine concentration.

Fig. S8. Pixel-to-pixel variation of PL.

Legends for movies S1 to S3

Other Supplementary Material for this manuscript includes the following:

(available at advances.sciencemag.org/cgi/content/full/5/11/eaat9476/DC1)

Movie S1 (.avi format). Visualizing ferrocenium diffusion using a MoS₂ pixel array.

Movie S2 (.avi format). Visualizing laminar flow of ions in a microfluidic channel.

Movie S3 (.avi format). Visualizing electroosmotic flow of ions in a microfluidic channel.

Supplementary Materials and Methods

1. Sample Fabrication

The monolayer MoS₂ films are directly grown on 1" transparent fused silica substrates using the Metal-Organic Chemical Vapor Deposition described in reference (28). The homogeneous coverage of monolayer MoS₂ was confirmed by atomic force microscopy and photoluminescence imaging. The film is patterned using UV-lithography techniques followed by SF₆/O₂ reactive ion etching at a power of 20 W. The contacts for the devices are defined using a second optical lithography step followed by e-beam evaporation of Ti/Au (5/50 nm).

Before measurements, the devices are treated by bis(trifluoromethane)-sulfonimide (TFSI) following the procedures described in reference (29). After the TFSI treatment the samples usually showed improved PL quantum efficiency by a factor of 2 to 10.

2. MoS₂ Characterization

A representative atomic force microscopy (AFM) image, fig. S1A shows continuous, monolayer MoS₂. The photoluminescence (PL) spectrum (fig. S1B) gives a peak at approximately 660 nm, consistent with previous results for MoS₂ on SiO₂ (1, 28, 29). The Raman spectrum (fig. S1C) also confirms the monolayer characteristics of our MoS₂ films.

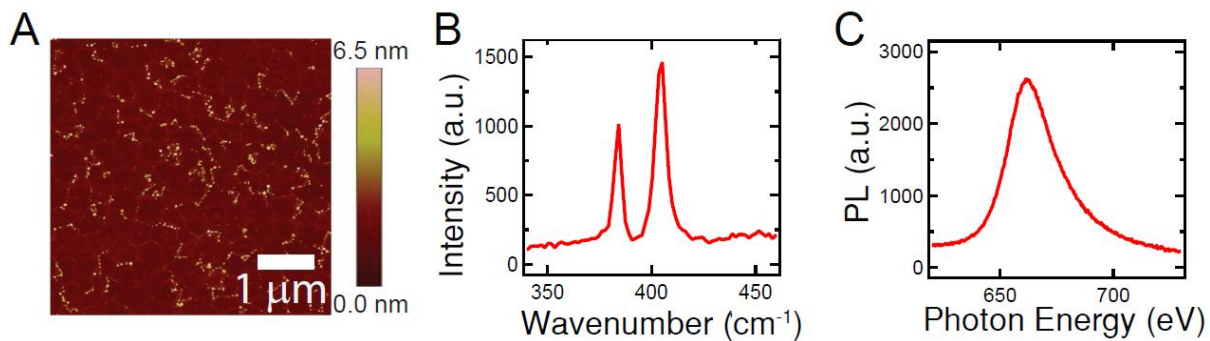


Fig. S1. Characterization of MoS₂ samples. (A) AFM of MoS₂ before patterning. (B) Raman spectrum of MoS₂ before patterning. (C) PL spectrum of patterned MoS₂.

3. Experimental Setup

The devices were measured using a probe-station with automated micromanipulators (Sensapex).

The samples were mounted with the MoS₂ side pointing up on an inverted microscope and imaged with a water immersion 60x objective with numerical aperture 1.25 and an Andor EM-CCD camera.

The PL measurements were made using a Hg arc lamp combined with a 550 nm bandpass filter (ThorLabs; 40 nm FWHM) and a dichroic mirror (Semrock; 552 nm long pass) as our incident light beam. The reflected light is partially filtered by the dichroic beamsplitter and further selected using a 650 nm bandpass filter (ThorLabs; 40 nm FWHM) which includes the A-exciton peak at room temperature (~ 660 nm). The setup schematics are shown in fig. S2.

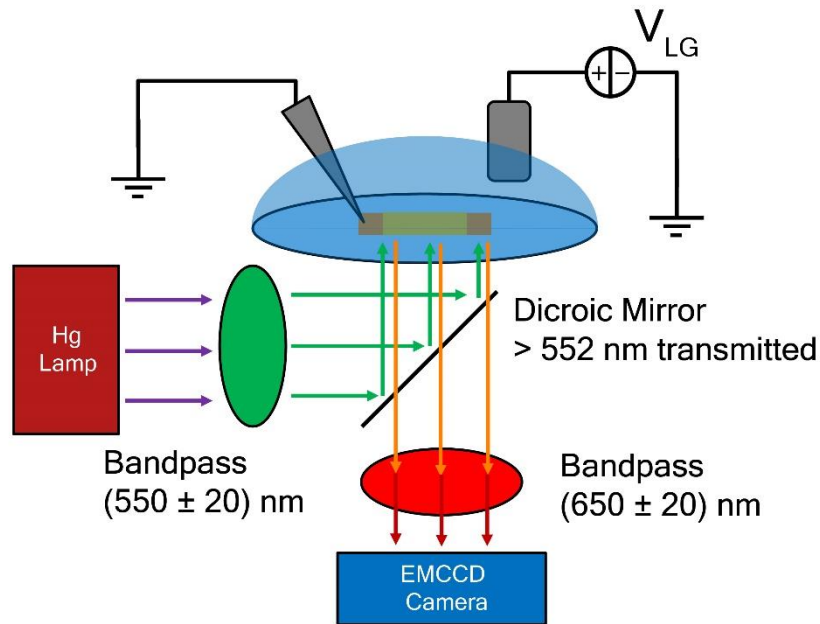


Fig. S2. Diagram of the experimental setup. The schematic shows the main elements as described in this section.

4. Relationship between carrier density and chemical potential

In general, the equation describing the potentials in the fluid can be written as

$$eV_{cir} = \mu_e(s) - \mu_e(m) \quad [1]$$

where V_{cir} is an applied potential between the solution and the MoS₂, and $\mu_e(s)$ and $\mu_e(m)$ are the electrochemical potentials of the solution and MoS₂ respectively. This equation can be expanded in terms of the chemical and electrostatic potentials of the solution and MoS₂, μ and ϕ

$$eV_{cir} = \mu_s - \mu_m + (\phi_s - \phi_m) \quad [2]$$

with subscripts s and m for solution and MoS₂ respectively.

In the case of a floating pixel, the applied voltage between the solution and the MoS₂ is zero. The electrostatic potential difference is maintained by the double layer capacitance at the interface, so we can rewrite the equation

$$\mu_s = \mu_m + \frac{ne^2}{C'} \quad [3]$$

where n is the electron doping per area and C' is the double layer capacitance per area. In the highly doped (degenerate) regime, the MoS₂ chemical potential is linear in doping: $\mu_m = n/g_{2D}$, where g_{2D} is the MoS₂ density of states. In the low doping (non-degenerate) limit, the chemical potential of MoS₂ is not linear in carrier density and can be written as

$$\mu_m = E + k_B T \ln \left(\frac{n}{g_{2D} k_B T} \right) \quad [4]$$

Plugging in for μ_m and differentiating μ_s with respect to n , we arrive at

$$\frac{d\mu_s}{dn} = \frac{k_B T}{n} + \frac{e^2}{C'} \quad [5]$$

We therefore expect that the relationship between chemical potential of the solution and doping of the MoS₂ should be linear either when $k_B T \ll \frac{ne^2}{C'}$ (electrostatic capacitance dominates in non-

degenerate limit) or when $k_B T \ll \frac{n}{g_{2D}}$ (chemical potential of MoS₂ is in the degenerate regime).

Since the electrostatic capacitance and quantum capacitance for MoS₂ in the degenerate regime are both on the order of 0.1 F/m^2 , for room temperature thermal energy we can safely assume that doping is linear in chemical potential when $n \gg 10^{12} \text{ cm}^{-2}$. This provides an explanation for the linear regime in the PL *versus* V_{LG} curve in Fig. 2B and 2C in the main text.

5. Experiments in Ruthenocene and Ruthenocene/Ferrocene mixtures

The detection of the electrochemical potential using the MoS₂ PL is not limited to ferrocene ions. In order to demonstrate this, we performed similar experiments as described in the main text with ruthenocene (C₁₀H₁₀Ru) in place of ferrocene. fig. S3A shows the MoS₂ PL and working electrode current as a function of the working electrode voltage for a solution of ruthenocene (500 μM). As with ferrocene, when the oxidation voltage of ruthenocene is reached ($V_W \sim 0.8 \text{ V}$) we see an increase in both I_W and the MoS₂ PL intensity.

The MoS₂ PL can also be used to detect ionic concentrations in solutions with two different molecules. By using a solution containing both ferrocene and ruthenocene with equal concentration (500 μM), we observe changes in the PL intensity at the oxidation voltages of both molecules (fig. S3B), showing that the optical detection of the ionic concentration, as the working electrode current in standard electrochemical cells, can be used for solutions of different molecules.

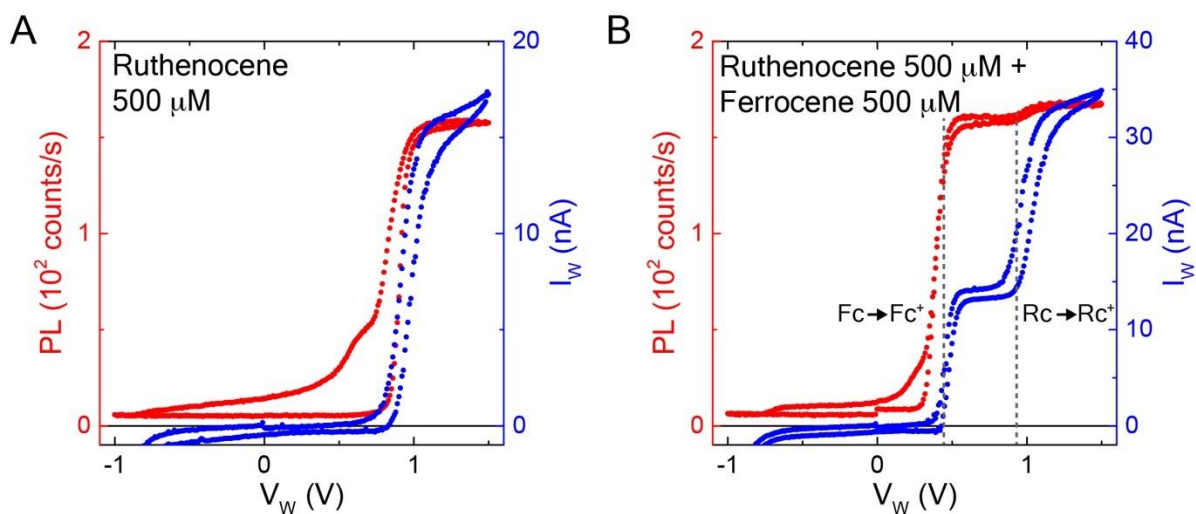


Fig. S3. Detection of ions in solutions containing ruthenocene and ruthenocene/ferrocene mixtures. (A) MoS₂ PL intensity and working electrode current (I_w) *versus* working electrode voltage (V_w) for a solution containing 500 μ M of ruthenocene. (B) PL and I_w *versus* V_w for a solution with ruthenocene (500 μ M) and ferrocene (500 μ M). The oxidation potentials for both molecules are indicated by the dashed gray lines.

6. Ionic current plots in diffusion experiments

PL measurements during diffusion can be used to plot concentration gradients by taking local gradients of PL. Using the same video shown in Fig. 3 of the main text, the PL of each pixel is plotted in a grid. Gradients are calculated at each point to determine the direction and magnitude of the arrows shown in fig. S4.

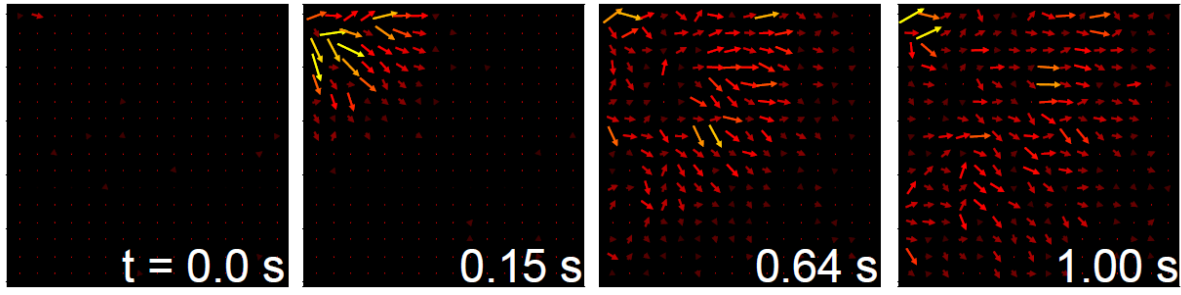


Fig. S4. Diffusion current mapping of ferrocene ions. Time series of images of the gradients of PL to represent the flow of ferrocenium away from the working electrode. The images are taken by calculating average PL at a MoS₂ pixel for each frame, finding the local gradient with respect to neighboring pixels, and averaging over four pixels to give the length and direction of each arrow.

7. Linear relationship between ferrocenium concentration and current

For simplicity, we model our ultramicroelectrode as a sphere, with a radius of approximately 10 μm . For oxidation of a molecule at a spherical ultramicroelectrode due to a potential step, steady state is reached when $t \gg \frac{r_0^2}{\pi D_0}$, where t is the time between the pulse and the measurement, r_0 is the radius of the electrode, and D_0 is the diffusion constant of the oxidized molecule (32). For our system, steady state is reached when the delay between potential step and measurement is much greater than 10 ms. For the CV measurements shown in the main text, delays between pulses and measurements were greater than 1 s, so our measurements were all taken in steady state.

In steady state, the relationship between concentration and current can be written

$$C_o = \left(\frac{D_R}{D_O} \right) C_R^* \left(\frac{i}{i_d} \right) \frac{r_0}{r} \operatorname{erfc} \left(\frac{r - r_0}{2(D_O t)^{1/2}} \right) \quad [6]$$

where C_O is the concentration of the oxidized molecule, C_R^* is the initial concentration of reduced molecules in the solution, i is the current and i_d is the limiting current, $erfc$ is the complementary error function, and r is the distance between the center of the sphere and a position in the solution (32). This equation shows that, if t remains the same for each measurement taken, the concentration of oxidized molecules at a fixed distance from the electrode is linearly proportional to the current measured at the electrode.

8. Decay time of MoS₂ PL as a function of concentration

While the PL of MoS₂ responds to redox molecules down to low (nanomolar) concentrations, the timescale of that response changes as a function of concentration. To demonstrate this, we set the potential of MoS₂ by contacting a microprobe to a device with gold pads and adjust the electrostatic potential such that the photoluminescence is discernably different from its steady-state floating value. After the electrical contact between the probe and the MoS₂ is deliberately broken, the PL transitions to the value set by the chemical potential of the solution containing ferrocene molecules. A set of time-lapsed images showing this decrease in PL is shown in fig. S6A. Plots of PL decay at four different concentrations are shown in fig. S6B. The decrease in decay time with increased concentration can be understood based on a simple RC-circuit model. R is the charge transfer resistance between the MoS₂ and solution, which decreases with increased concentration. C is the capacitance of the gold pads and MoS₂, which is roughly static with respect to changes in solution. However, the data are not fit well by a single exponential, which may be due to variation in the charge transfer rate as a function of doping of the MoS₂. Regardless, in lieu of plotting time constants, we plot the full width at half max of the decay time for each concentration measured (fig. S6C).

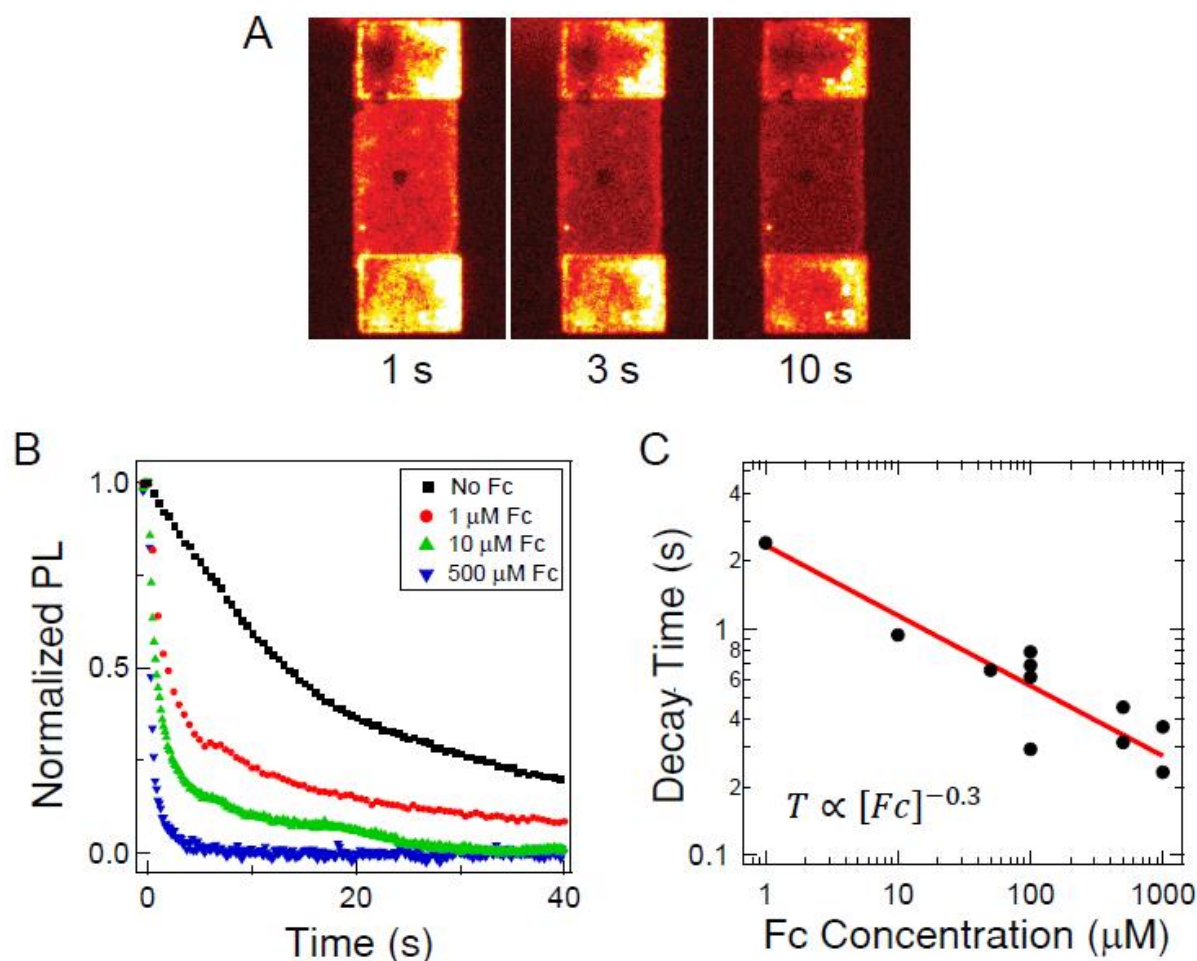


Fig. S5. PL decay time for varied Fc concentrations. (A) Time-lapse images of the photoluminescence of MoS₂ after breaking contact. (B) Normalized photoluminescence decay for contact breaking for different concentrations of ferrocene in solution. The time scale for decay decreases with increased concentration. Curves are fit with a double exponential to extract time constants. (C) Time constant *versus* concentration of ferrocene.

9. Electroosmotic Flow

In the same experimental setup as in Fig. 6A, B, we place two platinum wires on either side of the channel (fig S6A). By applying 50 V across the approximately 1 mm channel, we drive an electroosmotic flow. This flow is imaged with the MoS₂ PL in the same manner as before (fig. S6B), and shows a flat flow profile, in contrast to the parabolic flow profile for laminar flow.

Using the PL signal from the MoS₂ pixels, we calculate the velocity of the laminar and electroosmotic flows and plot the difference in velocity at a given position in the channel from the average velocity, depicting graphically the difference between laminar and electroosmotic flows as imaged by the MoS₂.

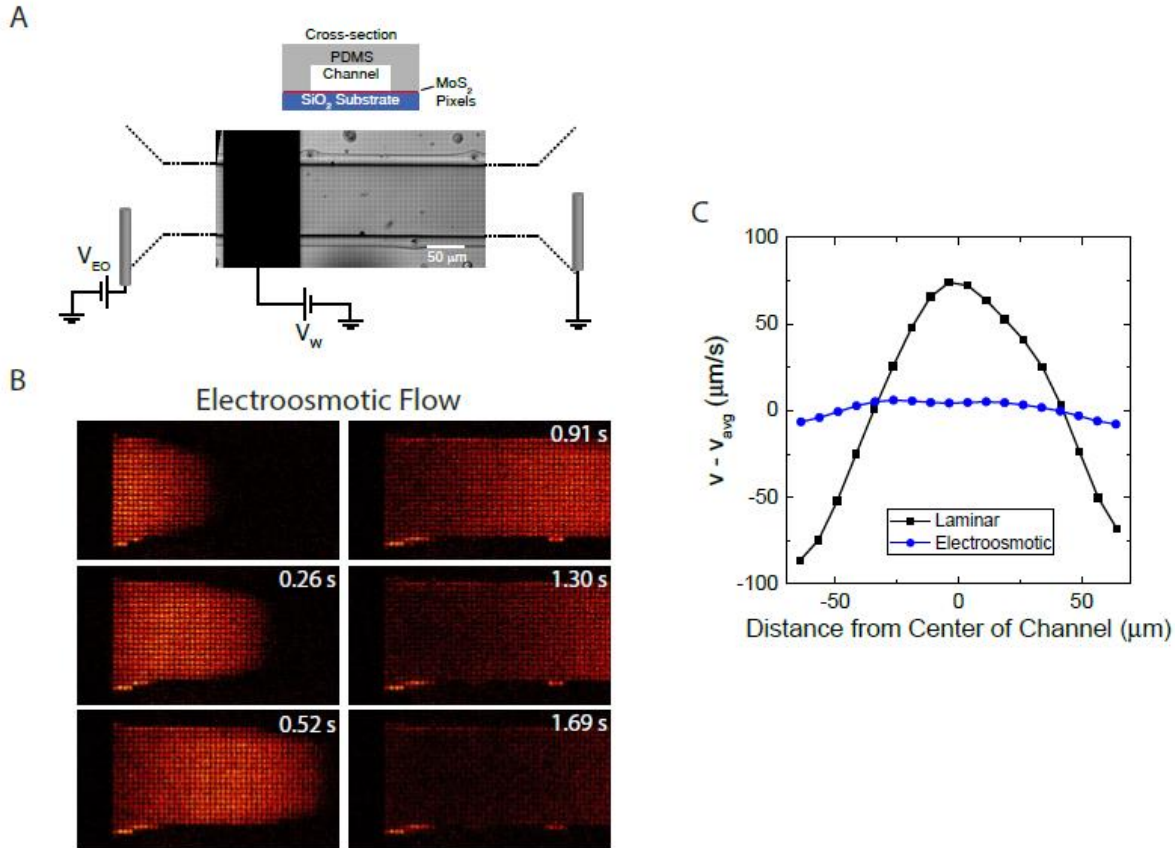


Fig. S6. PL imaging of electroosmotic flow. (A) Experimental setup for imaging of electroosmotic flow, showing the PDMS channel placed over the MoS₂ pixel array and surface electrode as before, with the addition of platinum electrodes on either side of the channel to drive the flow. (B) MoS₂ PL pixel imaging of electroosmotic flow, driven by a 50 V potential across the 1 mm channel length. (C) Plot of the velocity difference from average velocity across the width of the channel as calculated by the PL imaging for both electroosmotic and laminar flow, showing a flat profile for electroosmotic flow and a roughly parabolic profile for laminar flow.

10. Dopamine detection

We demonstrate that our detection scheme also works for redox biomolecules in aqueous solution by measuring PL *versus* dopamine concentration in a pH buffered solution, shown in fig. S7.

Without any dopamine in the solution, the MoS₂ is in a bright state at pH 5. Adding dopamine dopes the MoS₂ until the PL is off, as is expected since dopamine is an electron donor.

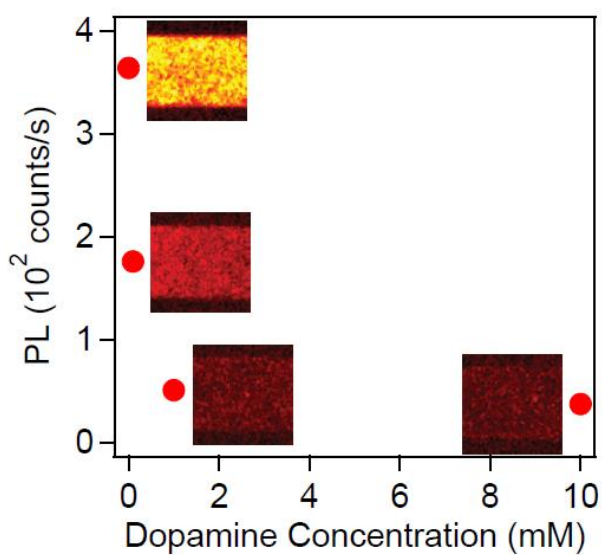


Fig. S7. PL versus dopamine concentration. PL *versus* dopamine concentration. Images correspond to adjacent data points.

11. PL Spatial Variation

In order to obtain some statistics on pixel-to-pixel variation in the PL intensity we can plot curves of the PL intensity versus changes in relative concentration of ferrocene and ferrocenium for several individual MoS₂ pixels. In doing so for 20 5x5 μm^2 pixels, we find well-correlated behavior and a standard deviation from the average pixel value of 6.5 %. These data indicate that the pixels are doped uniformly with respect to each other. The variance in PL values will add corresponding noise to any spatially resolved measurements in addition to any noise in the time domain, and the two noise sources are comparable for video frame rate measurements.

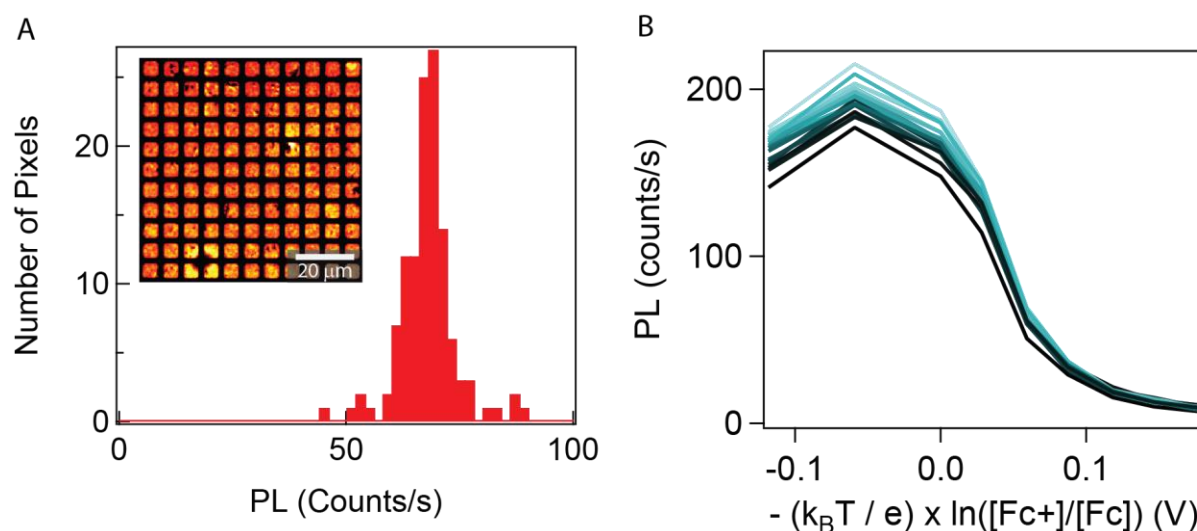


Fig. S8. Pixel-to-pixel variation of PL. (A) Histogram of PL values for an 11 by 11 array of 5 μm by 5 μm pixels. Inset: the pixel array from which the data were taken. The PL value is 68 counts/s and the standard deviation is 6 counts/s, corresponding to a 9% variation across the pixel array. A combination of damage to pixels, variation in illumination intensity from the mercury lamp, and spatial variation in MoS₂ PL contribute to the overall spatial variation of the array. (B) Traces of PL versus chemical potential for 20 5 μm by 5 μm pixels. Over the whole trace, the standard deviation of the pixel PL is 6.5% of the average pixel PL.

Movie S1. Visualizing ferrocenium diffusion using a MoS₂ pixel array. Real time video showing the response of a MoS₂ pixel array (2 μm x 2 μm) to the oxidation of ferrocene to ferrocenium and resultant diffusion of ferrocene along the array.

Movie S2. Visualizing laminar flow of ions in a microfluidic channel. Real time video of MoS₂ pixels responding to pressure-driven flow of a solution with ferrocene/ferrocenium molecules. At the beginning of the video, a platinum surface electrode oxidizes ferrocene to ferrocenium while flow in the channel is simultaneously driven by a syringe pump. The MoS₂ pixels turn on in response to the ferrocenium, imaging motion of the molecules down the channel.

Movie S3. Visualizing electroosmotic flow of ions in a microfluidic channel. Real time video of MoS₂ pixels responding to a voltage-driven flow of a solution with ferrocene/ferrocenium molecules. At the beginning of the video, a platinum surface electrode oxidizes ferrocene to ferrocenium while flow in the channel is simultaneously driven by an applied voltage of 50 V. The MoS₂ pixels turn on in response to the ferrocenium, imaging motion of the molecules down the channel.